1 1

Testing production scenarios for (anti-)(hyper-)nuclei with multiplicity-dependent measurements at the LHC

F. Bellini (CERN, Geneva) †
and A. P. Kalweit (CERN, Geneva)

The production of light anti- and hyper-nuclei provides unique observables to characterise the system created in high energy proton-proton (pp), proton-nucleus (pA) and nucleus-nucleus (AA) collisions. In particular, nuclei and hyper-nuclei are special objects with respect to non-composite hadrons (such as pions, kaons, protons, etc.), because their size is comparable to a fraction or the whole system created in the collision. Their formation is typically described within the framework of coalescence and thermal-statistical production models. In order to distinguish between the two production scenarios, we propose to measure the coalescence parameter B_A for different anti- and hyper-nuclei (that differ by mass, size and internal wave-function) as a function of the size of the particle emitting source. The latter can be controlled by performing systematic measurements of light anti- hyper- nuclei in different collision systems (pp, pA, AA) and as a function of the multiplicity of particles created in the collision. While it is often argued that the coalescence and the thermal model approach give very similar predictions for the production of light nuclei in heavy-ion collisions, our study shows that large differences can be expected for hyper-nuclei with extended wave-functions, as the hyper-triton. We compare the model predictions with data from the ALICE experiment and we discuss perspectives for future measurements with the upgraded detectors during the High-Luminosity LHC phase in the next decade.

1. Introduction: the "anti-nuclei" puzzle

The formation of light anti- and hyper-nuclei in high energy proton-proton (pp), proton-nucleus (pA) and nucleus-nucleus (AA) collisions provides unique observables for the study of the system created in these reactions, and can be used to understand both the internal structure and the formation mechanisms of loosely-bound composite objects. The production of (anti-)(hyper-)nuclei in high-energy collisions is commonly described

* XXV Cracow EPIPHANY Conference on Advances in Heavy Ion Physics
† Presenter. For correspondence: francesca.bellini@cern.ch

by following two distinct approaches: formation by nucleon coalescence at the system (kinetic) freeze-out [1–4] or thermal-statistical production at the chemical freeze-out [5,6]. Thanks to the large data samples of pp, p–Pb and Pb–Pb collisions collected during the first ten years of operations of the CERN Large Hadron Collider (LHC), A Large Ion Collider Experiment (ALICE) Collaboration has measured the production of light nuclei and anti-nuclei at several centre-of-mass energies [7–12], thus providing a crucial experimental input and a boost to theoretical and phenomenological investigations [13–19]. In small collision systems, the experimental results seem to confirm the validity of the coalescence picture, with the most recent multiplicity-differential measurements pointing toward a dependence of the coalescence process on the volume of the particle-emitting source ("source size" hereafter). In heavy-ion collisions, coalescence approaches that do not take into account the source size are not able to reproduce the data. At the same time, the production of light nuclei, anti-nuclei and hypertriton as measured in Pb–Pb collisions is found to be consistent with statistical-thermal model predictions and a non-zero deuteron elliptic flow is observed. This is surprising as (anti-)nuclei produced at chemical freeze-out are not expected to survive the hadronic phase: the deuteron is a "fragile object" when surrounded by the fireball created in heavy-ion collisions, because its binding energy ($B_E = 2.2$ MeV) is much lower than the characteristic temperatures of the system ($T_{chem} \approx 153$ MeV, $T_{kin} \approx 100$ MeV). Moreover, the cross-section for pion-induced deuteron breakup is significantly larger than the typical (pseudo)-elastic cross-sections for the re-scattering of hadronic resonance decay products [19–22]. These observations pose the "(anti-)nuclei puzzle": how can loosely-bound composite objects survive in the dense and hot fireball, freeze-out and develop collective flow like the other light-flavour non-composite hadrons?

In our study [14] we have extended and combined known formalisms used to describe (anti-)(hyper-)nuclei production in order to allow, for the first time, a direct comparison of the thermal and coalescence models as well as a direct comparison to the ALICE data. Identifying the coalescence parameter (B_A) as the key observable, we present a consistent picture across different collision systems (pp, p–Pb, Pb–Pb) for light (anti-)(hyper-)nuclei with mass number $A = 2, 3$ and 4. We also suggest to address the open questions by looking at the production of nuclei and hyper-nuclei up to $A = 4$ that differ by size and properties, measured as a function of multiplicity used as a proxy for the source size. Whereas the (anti-)deuteron production has been measured multi-differentially and quite precisely with the LHC Run 1 and 2 data, the study of heavier objects with $A = 3$ and 4 will greatly profit from the increase in integrated luminosity foreseen at the LHC Runs 3 and 4 in all collision systems [23]. A comprehension of (anti-)nuclei production

mechanisms is not only relevant for nuclear and hadronic physics, but has applications in astrophysics and indirect Dark Matter searches [24]. In recent years, it has been suggested that the detection of light anti-nuclei in space could provide a signature for the presence of Dark Matter in the Cosmos, see for instance [25, 26]. Anti-deuterons and $^3\overline{\mathrm{He}}$ might indeed be produced by coalescence of antiprotons and antineutrons coming from the annihilation of Weakly Interacting Massive Particles into Standard Model particles, for which anti-nuclei created in reactions between primary cosmic ray protons and interstellar matter (pp, pA collisions) represent a source of background.

The main features of the theoretical frameworks employed for our study are briefly summarised in Sec. 2, while we address the reader to [14] for the full details. Section 3 presents the main results and conclusions follow.

2. Modelling light (anti-)(hyper-)nuclei production

For our study, we consider nuclei and hyper-nuclei with mass number $A = 2, 3$ and 4, whose properties are summarised in Tab. 1. Those properties are the same as for their anti-matter counterparts and we assume that the same formation mechanisms are at play for matter and anti-matter[1]. Nuclei and hyper-nuclei are special objects with respect to non-composite hadrons (pions, protons, etc.), because their size is comparable to a fraction or the whole system created in pp, p–Pb and Pb–Pb collisions. The size is typically defined in two ways: a) as the rms of the (charge) distribution (λ_A), typically measured in electron scattering experiments, or b) as the size parameter of the object wave-function (r_A), typically taken as the gaussian solution of an isotropic harmonic oscillator potential in coalescence calculations. For light nuclei, $\lambda_A \approx 2$ fm. For the hyper-triton, theoretical calculations indicate a charge rms radius $\lambda_A \approx 5$ fm [27], driven by the average separation of the Λ relative to the two other nucleons. Assuming a similar structure (e.g. a s-wave interaction for a bound state of a n or a Λ with a deuteron), the hypertriton results in a much larger object than the other non-strange nuclei with $A = 3$. A simple relation holds between λ_A and r_A, see [14]. In Tab. 1 the binding energy (B_E) is also reported. The most tightly bound nucleus is ^{4}He, whereas the most loosely bound object is $^3_\Lambda$H, that is also the largest one. For the latter, we report the separation energy of the Λ baryon from the deuteron ($B_\Lambda = 0.13$ MeV). The large size and the low binding energy of the $^3_\Lambda$H with respect to the other (hyper-)nuclei has important consequences on its production, as discussed in what follows.

[1] For brevity, in the following we refer to "nuclei" and "hyper-nuclei" but we imply both matter and anti-matter.

Mass number	Nucleus	Composition	B_E (MeV)	Spin J_A	(Charge) rms radius ${\lambda_A}^{meas}$ (fm)	Harmonic oscillator size parameter r_A (fm)	Refs.
A = 2	d	pn	2.224575 (9)	1	2.1413 ± 0.0025	3.2	[28,29]
A = 3	^{3}H	pnn	8.4817986 (20)	1/2	1.755 ± 0.086	2.15	[30]
	^{3}He	ppn	7.7180428 (23)	1/2	1.959 ± 0.030	2.48	[30]
	$^{3}_{\Lambda}$H	pΛn	0.13 ± 0.05	1/2	4.9 – 10.0	6.8 – 14.1	[27,31]
A = 4	^{4}He	ppnn	28.29566 (20)	0	1.6755 ± 0.0028	1.9	[32,33]
	$^{4}_{\Lambda}$H	pΛnn	2.04 ±0.04	0	2.0 – 3.8	2.4 – 4.9	[27,31]
	$^{4}_{\Lambda\Lambda}$H	pΛΛn	0.39 – 0.51	1	4.2 – 7.1	5.5 – 9.4	[27]
	$^{4}_{\Lambda}$He	ppΛn	2.39 ± 0.03	0	2.0 – 3.8	2.4 – 4.9	[27,31]

Table 1. Properties of nuclei and hyper-nuclei with mass number $A \leq 4$. B_E is the binding energy in MeV. The size parameter r_A, is chosen to approximately reproduce the measured/expected rms, ${\lambda_A}^{meas}$ (fm). The proton rms charge radius $\lambda_p = 0.879(8)$ fm is subtracted quadratically from the measured rms charge radius λ_A^{meas} of the nucleus $\lambda_A = \sqrt{(\lambda_A^{meas})^2 - \lambda_p^2}$ to account for the finite extension of the constituents. Implicitly we assume here that $\lambda_\Lambda \approx \lambda_n \approx \lambda_p$.

2.1. The coalescence approach

In the coalescence picture, nucleons produced in the collision coalesce into nuclei if they are close in space and have similar velocities [1–3]. The coalescence probability is encoded in the coalescence parameter, B_A. Considering that at LHC energies the number of produced protons and neutrons at midrapidity as well as their momentum distributions are expected to be equal, B_A is defined as

$$E_A \frac{\mathrm{d}^3 N_A}{\mathrm{d}p_A^3} = B_A \left(E_{\mathrm{p,n}} \frac{\mathrm{d}^3 N_{\mathrm{p,n}}}{\mathrm{d}p_{\mathrm{p,n}}^3} \right)^A \Bigg|_{\vec{p}_{\mathrm{p}} = \vec{p}_{\mathrm{n}} = \frac{\vec{p}_A}{A}} , \tag{1}$$

where $p_{\mathrm{p,n}}$ are the proton and neutron momenta and $E_{p,n}$ their energies. Equation 1 represents also the operative definition of B_A that is used by experiments like ALICE to extract the coalescence probability starting from the measured nucleus and nucleon (proton) distributions. Starting from the model described in [3, 4], we have obtained in [14] a generalised expression for B_A

$$B_A = \frac{2J_A + 1}{2^A} \frac{1}{\sqrt{A}} \frac{1}{m_T^{A-1}} \left(\frac{2\pi}{R^2 + (\frac{r_A}{2})^2} \right)^{\frac{3}{2}(A-1)} , \tag{2}$$

which is a function of the spin of the particle J_A, its transverse mass m_{T}, its size parameter r_A and the source radius R. Very importantly, Eq. 2

takes explicitly into account the source size (R), as the coalescence probability naturally decreases for nucleons with similar momenta that are produced far apart in configuration space. Moreover, the source size is identified with the effective sub-volume of the whole system that is governed by the (momentum-dependent) homogeneity length of the interacting nucleons and experimentally accessible with Hanbury-Brown-Twiss (HBT) interferometry [3, 4]. Figure 1 shows the source radius dependence of B_A for nuclei and hyper-nuclei with $A = 2, 3$ and 4 whose properties are reported in Tab. 1. For the cases in which more than one estimate for r_A is available, we have adopted the lowest value for the calculations in Fig. 1. We observe that the

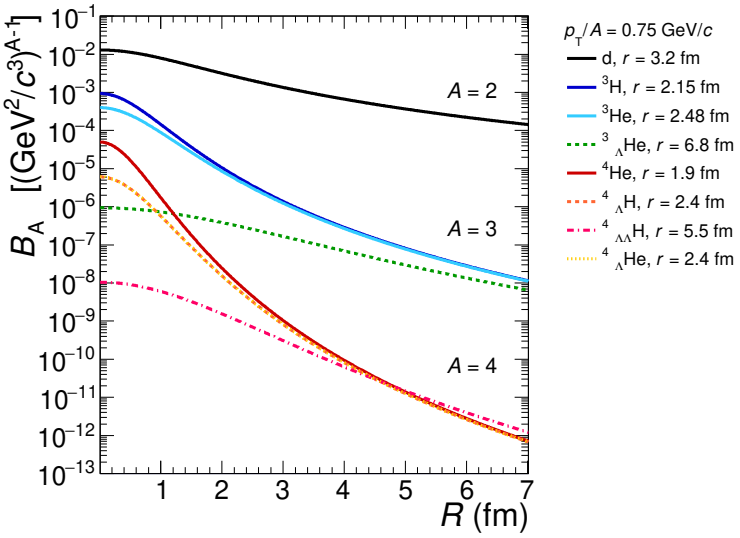

Fig. 1. (Color online) Coalescence parameter B_A as a function of the source radius R as predicted from the coalescence model (Eq. 2) for various composite objects with $p_T/A = 0.75$ GeV/c. For each (hyper-)nucleus, the radius r used for the calculation is reported in the legend.

coalescence probability decreases with increasing mass number and B_A decreases with increasing volume. For a given A, the larger the object radius, the lower is B_A, as clearly visible by comparing ^{3}He and $^3_\Lambda$H. For objects with same A, mass and spin (e.g. the isobars ^{3}H and ^{3}He), B_A differs only due to the different radius r_A. This difference is more relevant in small systems, because in large systems the difference between nucleus radii is much smaller than the size of the source. Incidentally, this could be experimentally verified with high precision measurements of the production of ^{3}H relative

to ^{3}He in pp collisions. The production of objects with radius larger than the source is strongly suppressed, indicating that the process is driven by the lenght scale defined by the object radius relative to the source radius.

2.2. Thermal + blast-wave model

Thermal-statistical models [5, 6] have been successful in describing the production of light (anti-)(hyper-)nuclei across a wide range of energies in AA collisions, including production at the LHC. In this approach, particles are produced from a fireball in thermal equilibrium with temperatures of $T_{chem} \approx 156$ MeV. Particle yields are derived from the partition function assuming a Grand Canonical ensemble[2] and they depend only on the mass of the particle and the temperature of chemical freeze-out, $\mathrm{d}N/\mathrm{d}y \propto \exp(-m/T_{\mathrm{chem}})$. The thermal model cannot – alone – be compared to the p_{T}-dependent coalescence description because it provides only predictions for p_{T}-integrated yields. A thermal particle production implies a Boltzmann distribution of the momenta only for a static source, which is not the case of the rapidly expanding system produced in heavy-ion collisions. The thermal model (i.e. the GSI-Heidelberg implementation we have considered here) needs to be complemented by a hydrodynamic description of the rapidly expanding source. To that end, we use the Blast-Wave model [35], which has been proven to describe reasonably well the measured momentum distributions of protons [36]. Our "thermal+blast-wave" approach results from the combination of the two models: the p_{T}-dependence is modelled by the blast-wave whereas the normalisation (i.e. the p_{T}-integrated yield) is taken from the thermal model predictions.

3. Comparison with data

[2] Extensions to small systems employ a canonical ensemble partition function to account for the exact conservation of quantum numbers in a finite size system, see for instance [34].

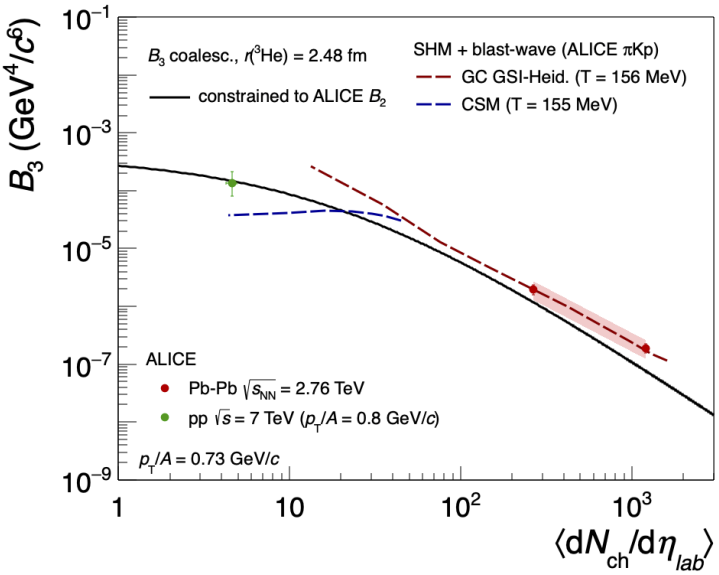

Fig. 2. (Color online) Coalescence parameter B_3 for ^{3}He as a function of the average charged particle multiplicity density. The coalescence calculation (continuous black line) is compared to two thermal+blast-wave predictions (dashed lines), obtained by using the Grand Canonical (GC, red) [6] and Canonical Statistical Model (CSM, blue) [34] expectations for the ^{3}He yield, respectively. ALICE data from pp (green circles) and Pb–Pb (red circles) collisions [7, 9] are reported.

REFERENCES

[1] S. T. Butler and C. A. Pearson *Phys. Rev.* **129** (1963) 836–842.

[2] J. I. Kapusta *Phys. Rev.* **C21** (1980) 1301–1310.

[3] R. Scheibl and U. W. Heinz *Phys. Rev.* **C59** (1999) 1585–1602, `arXiv:nucl-th/9809092 [nucl-th]`.

[4] K. Blum, K. C. Y. Ng, R. Sato, and M. Takimoto *Phys. Rev.* **D96** no. 10, (2017) 103021, `arXiv:1704.05431 [astro-ph.HE]`.

[5] A. Andronic, P. Braun-Munzinger, J. Stachel, and H. Stocker *Physics Letters B* **697** no. 3, (2011) 203 – 207.

[6] A. Andronic, P. Braun-Munzinger, K. Redlich, and J. Stachel *Nature* **561** no. 7723, (2018) 321–330, `arXiv:1710.09425 [nucl-th]`.

[7] **ALICE** Collaboration, J. Adam *et al. Phys. Rev.* **C93** no. 2, (2016) 024917, `arXiv:1506.08951 [nucl-ex]`.

[8] **ALICE** Collaboration, J. Adam *et al. Phys. Lett.* **B754** (2016) 360–372, `arXiv:1506.08453 [nucl-ex]`.

[9] **ALICE** Collaboration, S. Acharya *et al. Phys. Rev.* **C97** no. 2, (2018) 024615, arXiv:1709.08522 [nucl-ex].

[10] **ALICE** Collaboration, S. Acharya *et al. Eur. Phys. J.* **C77** no. 10, (2017) 658, arXiv:1707.07304 [nucl-ex].

[11] **ALICE** Collaboration, M. Puccio *Nucl. Phys.* **A982** (2019) 447–450.

[12] **ALICE** Collaboration, S. Acharya *et al.* arXiv:1902.09290 [nucl-ex].

[13] S. Mrowczynski *Acta Phys. Polon.* **B48** (2017) 707, arXiv:1607.02267 [nucl-th].

[14] F. Bellini and A. P. Kalweit arXiv:1807.05894 [hep-ph].

[15] S. Bazak and S. Mrowczynski *Mod. Phys. Lett.* **A33** no. 25, (2018) 1850142, arXiv:1802.08212 [nucl-th].

[16] W. Zhao, L. Zhu, H. Zheng, C. M. Ko, and H. Song *Phys. Rev.* **C98** no. 5, (2018) 054905, arXiv:1807.02813 [nucl-th].

[17] K.-J. Sun, C. M. Ko, and B. Doenigus arXiv:1812.05175 [nucl-th].

[18] X. Xu and R. Rapp arXiv:1809.04024 [nucl-th].

[19] D. Oliinychenko, L.-G. Pang, H. Elfner, and V. Koch arXiv:1809.03071 [hep-ph].

[20] H. Garcilazo *Phys. Rev. Lett.* **48** (1982) 577–580.

[21] S. A. Bass *et al. Prog. Part. Nucl. Phys.* **41** (1998) 255–369, arXiv:nucl-th/9803035 [nucl-th].

[22] J. Schukraft *Nucl. Phys.* **A967** (2017) 1–10, arXiv:1705.02646 [hep-ex].

[23] Z. Citron *et al.* in *HL/HE-LHC Workshop: Workshop on the Physics of HL-LHC, and Perspectives at HE-LHC Geneva, Switzerland, June 18-20, 2018*. 2018. arXiv:1812.06772 [hep-ph].

[24] T. Aramaki *et al. Phys. Rept.* **618** (2016) 1–37, arXiv:1505.07785 [hep-ph].

[25] M. Cirelli, N. Fornengo, M. Taoso, and A. Vittino *JHEP* **08** (2014) 009, arXiv:1401.4017 [hep-ph].

[26] M. Korsmeier, F. Donato, and N. Fornengo *Phys. Rev.* **D97** no. 10, (2018) 103011, arXiv:1711.08465 [astro-ph.HE].

[27] H. Nemura, Y. Suzuki, Y. Fujiwara, and C. Nakamoto *Prog. Theor. Phys.* **103** (2000) 929–958, arXiv:nucl-th/9912065 [nucl-th].

[28] C. Van Der Leun and C. Alderliesten *Nucl. Phys.* **A380** (1982) 261–269.

[29] P. J. Mohr, D. B. Newell, and B. N. Taylor *Rev. Mod. Phys.* **88** no. 3, (2016) 035009, arXiv:1507.07956 [physics.atom-ph].

[30] J. E. Purcell and C. G. Sheu *Nucl. Data Sheets* **130** (2015) 1–20.

[31] D. H. Davis *Nucl. Phys.* **A754** (2005) 3–13.

[32] M. Wang, G. Audi, F. Kondev, W. Huang, S. Naimi, and X. Xu *Chinese Physics C* **41** no. 3, (2017) 030003.

[33] I. Angeli and K. P. Marinova *Atom. Data Nucl. Data Tabl.* **99** no. 1, (2013) 69–95.

225 [34] V. Vovchenko, B. Doenigus, and H. Stoecker *Phys. Lett.* **B785** (2018)
226 171–174, arXiv:1808.05245 [hep-ph].
227 [35] E. Schnedermann, J. Sollfrank, and U. W. Heinz *Phys. Rev.* **C48** (1993)
228 2462–2475, arXiv:nucl-th/9307020 [nucl-th].
229 [36] **ALICE** Collaboration, B. Abelev *et al. Phys. Rev.* **C88** (2013) 044910,
230 arXiv:1303.0737 [hep-ex].

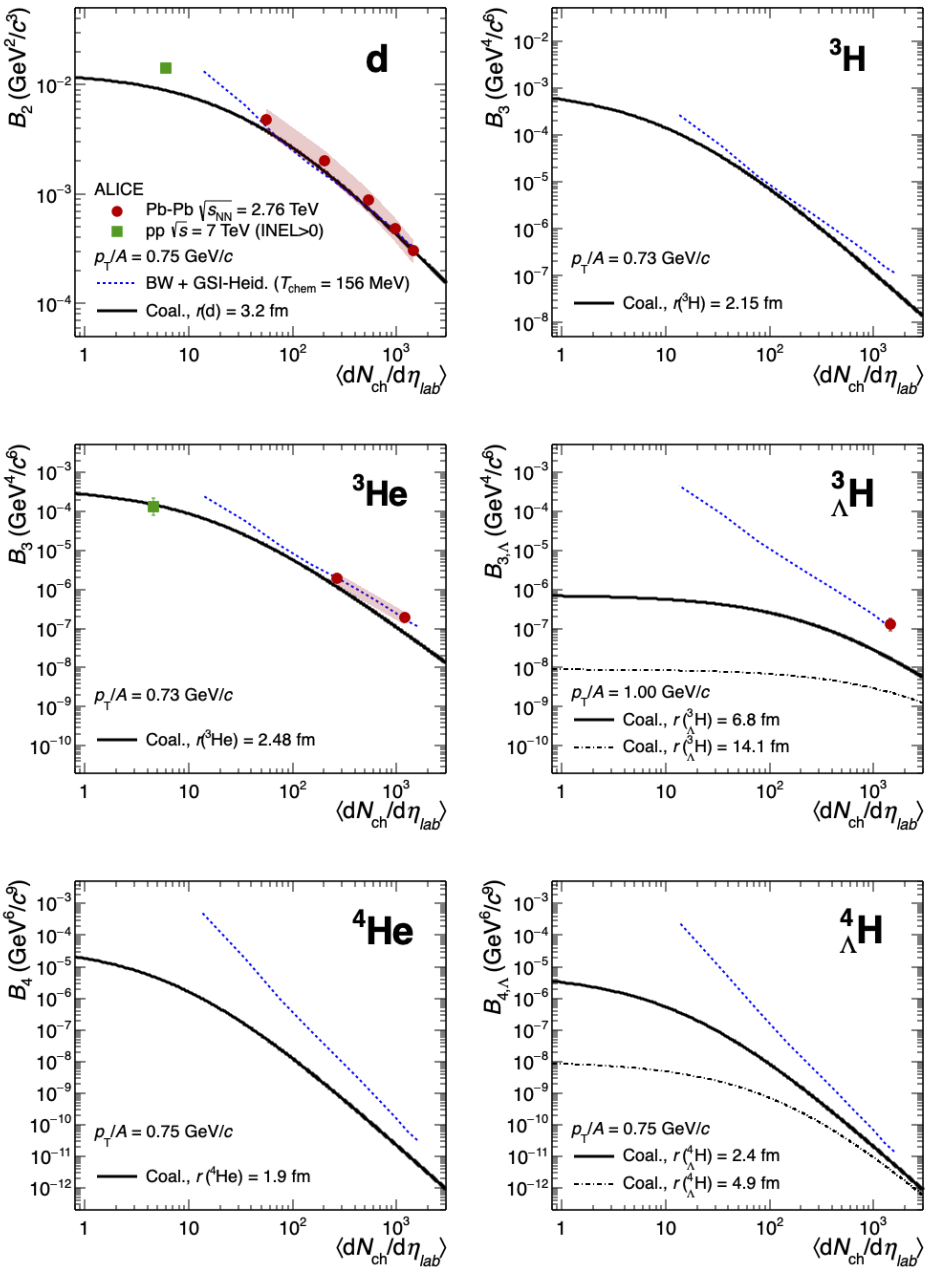

Fig. 3. (Color online) Coalescence parameter B_A as a function of the average charged particle multiplicity density for various (hyper-)nuclei, up to $A = 4$. The coalescence calculations (continuous or dashed-dotted black lines) are compared to the thermal+blast-wave predictions (dashed blue line), as well as to pp (green square) and Pb–Pb (red circles) collision data from ALICE [7–9].